S_E2 reaction in noncarbon system: Metal-halide catalysis for dehydrogenation of ammonia borane

Sung Jin Pai (배성진)[a] and Sang Soo Han (한상수)[a,1]

[a]Computational Science Research Center, Korea Institute of Science and Technology, Seongbuk-gu, Seoul 136-791, Republic of Korea

Edited by Jerrold Meinwald, Cornell University, Ithaca, NY, and approved November 15, 2017 (received for review July 7, 2017)

An electrophilic substitution (S_E) reaction of BN isosteres has been investigated for the dehydrogenation of ammonia borane (AB) by metal chlorides (MCl_2) using various ab initio calculations. In contrast to the typical S_E reaction occurring at the carbon atom, the nitrogen atom in AB serves as the reaction center for the S_E reaction with the boron moiety as the leaving group when the MCl_2 approaches the AB. The S_E2 backside reaction is favored as a trigger step for the dehydrogenation of AB by the MCl_2. The S_E2 reaction is found for 3d-transition-metal chlorides (e.g., $FeCl_2$, $CoCl_2$, $NiCl_2$, $CuCl_2$, and $ZnCl_2$), while $PdCl_2$ leads to the dehydrogenation of AB by a direct B–H σ-bond activation, similar to most organometallic catalysts. Interestingly, the polymerization of AB promoted by MCl_2 can be explained with the similar S_E2 mechanism, and the dehydrogenation of the BN derivative 3-methyl-1,2-BN-cyclopentane (CBN) bearing a carbon backbone ring also follows the S_E2 reaction. In particular, the experimental observation that the use of metal-chloride catalysis decreases the by-products obtained during the hydrogenation of AB can be explained by our mechanism involving the S_E2 reaction. This work is helpful for the development of novel metal-halide catalysts for practical hydrogen storage materials, including the BN moiety.

S_E2 reaction | hydrogen storage | ammonia borane | catalyst | ab initio

Substitution reactions, a class of chemical reactions in which one functional group in a chemical compound is replaced by another functional group, are ubiquitous in organic chemistry (https://en.wikipedia.org/wiki/Substitution_reaction). Substitution reactions are classified either as nucleophilic (S_N) or electrophilic (S_E), depending on the underlying mechanism. Although S_E reactions are less common than S_N reactions, the S_E reaction mechanism is more complicated, indicating that the variation among these processes is wider, which in turn means that there is a higher probability of unknown reactions (1–5). Therefore, whereas the S_N reaction has been usually observed in carbon systems, the S_E reaction would be able to occur in noncarbon systems.

Recently, ammonia borane (AB) has received significant attention as a promising onboard hydrogen storage material for use in transportation due to its high hydrogen storage capacity (19.6 wt % H_2) (6–9). There has been considerable effort to lower the operating temperature for fuel cells to 80 °C; consequently, homogeneous catalysis has become a promising alternative means of lowering the activation energy barrier of the dehydrogenation reaction pathway (10–17). In particular, organometallic catalysts lower the dehydrogenation barrier of AB by the coordination of the hydrogen atoms bonded to boron or nitrogen to the metal centers of the catalyst (16), where the coordination activates the B–H or N–H bond, followed by hydrogen transfer to the metal center or ligands. Recently, the dehydrogenation mechanism of AB and amine borane by various complex metal hydrides has been thoroughly reviewed by Rossin and Peruzzini (18). As more cost-effective promoters than organometallic catalysts, metal halides have been considered as homogeneous catalysts for AB dehydrogenation (19–21). Homogeneous metal-halide catalysis has also been applied to improve the dehydrogenation of 3-methyl-1,2-BN-cyclopentane (CBN), which is a promising liquid-phase H_2 storage material (22). For catalytic reactions with metal halides, it has been suggested that similar to the case of organometallic catalysis, the metal cation in metal halides initiates AB dehydrocoupling and retains a B–N unit during AB dehydrogenation (19, 20); however, the details of this proposed mechanism have not been investigated further.

While extending our search for an optimal metal-halide catalyst for the efficient dehydrogenation of AB, we have thoroughly explored the reaction pathway and kinetics of the dehydrogenation process using ab initio calculations. These efforts have led to the finding that an S_E2 reaction occurs between the metal center and AB at the initial step of dehydrogenation and determines the performance of metal-halide catalysts, showing the possibility of an S_E2 reaction in a noncarbon system. In contrast to previous S_E reactions, the possibility of such a reaction on the B–N unit in an AB molecule can provide an opportunity for BN isostere chemistry, particularly with regard to the replacement of two carbon atoms (C–C) by the B–N moiety to produce various structures with interesting electronic structure and chemistry (23–27). In this work, the catalytic effects of various metal halides in the S_E2 reaction for AB dehydrogenation are explored by several ab initio calculations, and their catalytic activity is discussed on the basis of quantum-mechanical energetics and molecular orbital (MO) analysis. Our calculations are also supported by a comparison with previous experimental results. Furthermore, it is confirmed that a similar S_E2 mechanism is also applicable to catalysis for the CBN system, which has been recently reported as a potential hydrogen storage medium (22).

Results and Discussion

Direct Hydrogen Activation. According to a previous study (28) of organometallic catalysts for AB dehydrogenation, the dehydrogenation reaction occurs through the activation of a B–H or N–H bond at a metal center. Thus, for the metal-halide catalysts considered in

Significance

Ammonia borane (AB) is a promising hydrogen storage material due to its high hydrogen storage capacity. AB dehydrogenation can be facilitated by metal-halide (MCl_2) catalysis. Here, we have elucidated the dehydrogenation mechanism of AB via MCl_2 catalysis using ab initio calculations. In contrast to a typical electrophilic substitution (S_E) reaction occurring at a carbon atom, the nitrogen atom in AB serves as the reaction center for the S_E reaction with the boron moiety as the leaving group when MCl_2 approaches AB. In addition, the S_E2 backside reaction is favored as the initial step for the dehydrogenation of AB by MCl_2. This work paves the way for the use of a new reaction in the field of BN chemistry.

Author contributions: S.S.H. designed research; S.J.P. performed research; S.J.P. and S.S.H. contributed new reagents/analytic tools; S.J.P. and S.S.H. analyzed data; and S.J.P. and S.S.H. wrote the paper.

The authors declare no conflict of interest.

This article is a PNAS Direct Submission.

[1]To whom correspondence should be addressed. Email: sangsoo@kist.re.kr.

This article contains supporting information online at www.pnas.org/lookup/suppl/doi:10.1073/pnas.1712137115/-/DCSupplemental.

this work, we first investigated the dehydrogenation mechanism occurring through B–H activation, similar to the behavior observed in the case of organometallic catalysts. *SI Appendix*, Fig. S1 shows the AB dehydrogenation reaction pathways via B–H activation of metal chlorides, where $FeCl_2$ and $PdCl_2$ are used as representatives of 3d- and 4d-metal halides, respectively. For $FeCl_2$ (*SI Appendix*, Fig. S1*A*), the iron atom binds with two σ-B–H bonds in the AB molecule with a binding energy of 29.6 kcal/mol. However, a careful investigation reveals that no further reactions occur. This indicates that the dehydrogenation via B–H activation is not favorable, in contrast to the experiments (21, 29) reporting that $FeCl_2$ can promote the dehydrogenation of AB. We also investigated other 3d-metal halides, such as $CoCl_2$, $NiCl_2$, $CuCl_2$, and $ZnCl_2$, and found that similar to the $FeCl_2$ case, these metal halides cannot activate the B–H bond.

On the other hand, $PdCl_2$ can activate a B–H bond in AB (*SI Appendix*, Fig. S1*B*). $PdCl_2$ interacts with one σ-B–H bond, that B–H bond is shifted toward a neighboring H atom, and then a H_2 molecule is released in a step with an energy barrier of 12.9 kcal/mol. According to a previously reported experiment (21), the grinding of AB and $PdCl_2$ does indeed lead to H_2 generation. It is expected that the dehydrogenation reaction would occur via the mechanism shown in *SI Appendix*, Fig. S1*B*. This difference between $FeCl_2$ and $PdCl_2$ results from the fact that Fe^{2+} is a hard acid, while both Pd^{2+} and BH_3 are soft acids (30). Thus, $PdCl_2$ and BH_3 can interact more readily than $FeCl_2$ and BH_3.

S_E2 Reaction at a B–N Unit. Although our calculations indicate that direct B–H activation in AB by nonprecious metal halides is not favorable, several experiments reported their catalytic activity (19–21, 29), implying the possibility of an alternative route for the dehydrogenation of AB via MCl_2. The electropositive nature of the metal centers in the metal halides and the electron-rich nature and attachment to a potential leaving group, BH_3, of the nitrogen atom in AB support the occurrence of an S_E-type reaction in the AB and MCl_2 system for AB dehydrogenation, especially for the occurrence of an S_E2-type pathway over an S_E1-type pathway.

Although the S_N2 reaction occurs mostly through one route with rare exceptions (31), S_E2 reactions can proceed through various routes (2). Since there is no severe steric hindrance at the NH_3 or BH_3 group in AB, two plausible pathways for the MCl_2 + AB system can be considered: (*i*) the front-side open-retention pathway, S_E2(FS), and (*ii*) the backside inversion pathway, S_E2(BS). Fig. 1 shows the S_E2(FS) and S_E2(BS) pathways for $FeCl_2$ + AB system as calculated at the density-functional theory (DFT) with a dispersion correction for two-body energy (D2) level of theory. We have confirmed that the DFT-D2 reaction energies are similar to the coupled-cluster singles and doubles plus perturbative triples [CCSD(T)] energies, as shown in *SI Appendix*, Fig. S3. For the S_E2(FS) pathway, the Fe atom in $FeCl_2$ approaches the B–N bond, leading to an increase in the length of B–N bond from 1.63 to 2.80 Å, a reaction that is uphill by 15.9 kcal/mol and has an energy barrier of 16.6 kcal/mol. At the final state, full dissociation of the B–N bond did not occur because the H atom in BH_3 is bound to the Fe atom by electrostatic interactions. A further reaction does not occur, indicating that the S_E2 (FS) reaction does not lead to the dehydrogenation of AB.

On the other hand, for the S_E2(BS) reaction, the Fe metal center in $FeCl_2$ attacks the N atom in AB through the backside route, followed by the BH_3 group leaving. The transition state (TS) for the reaction involves an inversion of the tetrahedral geometry at the N center, as observed in typical substitution reactions. The calculated energy barrier is 5.7 kcal/mol, much lower than that for the S_E2(FS) route. Moreover, the reaction is slightly downhill. After the S_E2 reaction, an additional process involving the recombination of the B–N bond can occur due to the absence of steric or rotational hindrance between the two dissociated groups. The second activation energy for the dehydrogenation is 20.8 kcal/mol, much lower than that for AB in the absence of a catalyst (34.2 kcal/mol). A long distance (2.87 Å) between the Fe–N moiety and the BH_3 leaving group is the origin of the barrier-lowering effect, while in the noncatalyst case, a considerable contribution of the activation energy results from repulsion inducing the rotation and bending of the N and B atoms in AB (32, 33). Here, BH_3 can be an intermediate product during the dehydrogenation reaction of MCl_2 + AB. However, because BH_3 itself is a very active species, it combines with another BH_3 to dimerize into B_2H_6. According to a previous experiment (29), B_2H_6 was indeed observed as a by-product during the

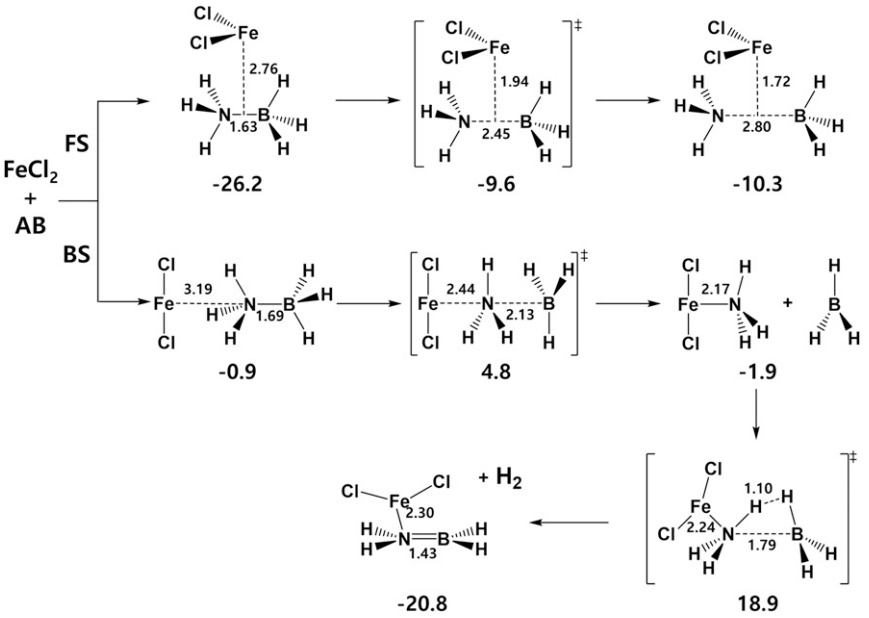

Fig. 1. Two plausible S_E2 reaction pathways for AB dehydrogenation with the help of $FeCl_2$. Upper and lower routes are S_E2(FS) and S_E2(BS), respectively. Numerical values in each structure are relative energies (in kilocalories per mole) to separate $FeCl_2$ and AB as a reference. In each structure, the B–N and M–N distances in angstroms are included.

Table 1. Comparison of the calculated energy barriers for AB dehydrogenation by various MCl_2

MX_n	S_E2(BS)	RC_{BN}	$\Delta E^{(2)}{}_{N \rightarrow B^*}$	$\Delta E_{\Pi u^*}$
$FeCl_2$	6.9	22.1	19.6	6.9
$CoCl_2$	10.9	19.9	29.7	8.2
$NiCl_2$	8.3	20.5	30.6	7.5
$CuCl_2$	4.0	20.7	32.4	5.6
$ZnCl_2$	13.0	19.8	15.9	8.2

Mechanism is similar to that shown in Fig. 1 and *SI Appendix*, Fig. S3. Dehydrogenation is a two-step reaction including the S_E2(BS) and the recombination of B–N bond (RC_{BN}). The energy barrier value is relative to the isolated AB and MCl_2. The energy difference ($\Delta E_{\Pi u^*}$) between the π_u^* MO level of single MCl_2 and the HOMO level at the TS for the S_E2 reaction is also compared. The energies are obtained at the calculation level of CCSD(T). All energies are in kilocalories per mole.

dehydrogenation reaction of AB with various MCl_2 catalysts (e.g., $FeCl_2$, $CoCl_2$, $NiCl_2$ $CuCl_2$, and $ZnCl_2$). This result clearly supports our S_E2 mechanism.

Comparison of Various Metal-Halide Catalysts for the Dehydrogenation of AB. At this point, it is plausible that the catalytic reaction pathway through the S_E2(BS) route using $FeCl_2$ lowers the energy barrier to 20.8 kcal/mol (Fig. 1), enabling the reaction to proceed near 80 °C. However, according to an experimental report (29), not all metal halides are effective for the dehydrogenation of AB, and the catalyst efficiency is correlated with the intrinsic properties of the metal center, such as electronegativity. Although a higher electronegativity generally leads to more efficient catalysis, several exceptions to this rule are found for the first-row transition metals. For example, the electronegativities of Co and Ni are higher than that of Fe; however, their catalytic efficiencies are lower than that of Fe (29). Therefore, we need to further explore the dehydrogenation process involving the S_E2(BS) reaction pathway for various metal halides.

Using CCSD(T) calculations, we investigated reaction pathways involving the S_E2(BS) reaction for AB dehydrogenation by several first-row transition-metal chlorides ($FeCl_2$, $CoCl_2$, $NiCl_2$, $CuCl_2$, and $ZnCl_2$) and compared their reaction energies in Table 1. The information is also summarized in more detail in *SI Appendix*, Table S2. Here, it is necessary to mention that the dehydrogenation process is a two-step reaction involving the S_E2(BS) mechanism and the recombination of the B–N bond (RC_{BN}). According to Table 1, the second step corresponding to the recombination reaction of the B–N bond is the rate-determining step for all first-row MCl_2; however, irrespective of the type of MCl_2, the relevant energy barrier is ∼20 kcal/mol. On the other hand, the first energy barrier concerning the S_E2 reaction is more sensitively affected by the identity of MCl_2. According to the reaction kinetics, the reaction rate for a two-step reaction (fast followed by slow) is proportional to $k_{slow}(k_{fast\_front}/k_{fast\_back})$ (34), indicating that the fast reaction can be a critical factor for the determination of the reaction rate in the case of similar energy barriers for slow reactions. Therefore, the S_E2 reaction can determine the AB dehydrogenation rate, even though the energy barrier for the S_E2 reaction is lower than that of the B–N bond recombination reaction. Experimentally (29), H_2 desorption peak temperatures from AB by the MCl_2 catalysts show the following trend: $ZnCl_2 > CoCl_2 \sim NiCl_2 > FeCl_2 > CuCl_2$, indicating that the $CuCl_2$ is the best candidate (Fig. 2). Indeed, this trend is well-correlated with the calculated S_E2 energy barrier, where the barrier order is $ZnCl_2 > CoCl_2 > NiCl_2 > FeCl_2 > CuCl_2$.

To confirm that the same mechanism for dehydrogenation of AB and metal halide also occurs in the solid state, periodic slab calculations were additionally performed, in which a nudged elastic band calculation (*SI Appendix*, Fig. S4) and a first-principles molecular dynamics simulation (*SI Appendix*, Fig. S5) were considered. The relevant computation details are described in *SI Appendix*. Indeed, both of the slab calculations clearly show that the dehydrogenation of AB involving the S_E2 reaction can still occur in solids of AB and a metal halide.

To elucidate the effects of the MCl_2 catalysts on the S_E2 reaction barrier, we have also investigated the MCl_2 electronic structures. Because this S_E2 reaction accompanies a charge transfer similar to a general donor–acceptor interaction, the second-order perturbation stabilization energies from i to j^* [$\Delta E^{(2)}{}_{i \rightarrow j^*}$] were calculated using a natural bonding orbital (NBO) method, in which the interaction between occupied and vacant orbitals is represented to stabilize the superposition of each orbital. From the calculation, we find that the TS energy for the S_E2 reaction is mainly determined by an intrinsic energy-lowering effect of the donor–acceptor interaction between a lone-pair orbital of nitrogen in AB and an unfilled lone-pair orbital of boron, as seen in *SI Appendix*, Fig. S8. Calculated $\Delta E^{(2)}{}_{N \rightarrow B^*}$ values are summarized in the third column of Table 1. A comparison of the $\Delta E^{(2)}{}_{N \rightarrow B^*}$ values between MCl_2 catalysts shows that the energy is higher for a metal with a larger electronegativity (Cu > Ni > Co > Fe > Zn). Moreover, the energy inversely correlates with the energy barrier of the S_E2 reaction, with the exception of $FeCl_2$. In other words, the $\Delta E^{(2)}{}_{N \rightarrow B^*}$ of $FeCl_2$ is expected to fall between those of $CuCl_2$ and $NiCl_2$ because the order of the S_E2 reaction barriers is $CuCl_2 < FeCl_2 < NiCl_2 < CoCl_2 < ZnCl_2$; however, it is in fact lower than those of $CoCl_2$ and $NiCl_2$. The exceptional case of $FeCl_2$ can be explained by another effect that is discussed below.

During the S_E2 reaction, a linear symmetry of the MCl_2 molecule is broken by interacting with the lone-pair orbital of the nitrogen atom (*SI Appendix*, Fig. S9), which reveals that the S_E2 energy barrier is also associated with an energy to retain this linear symmetry of the MCl_2 molecule. The π_{u^*} near the highest-occupied MCl_2 MO (HOMO) level has a suitable symmetry for the interaction with the AB MO, as seen in *SI Appendix*, Fig. S9. It can be inferred from the above discussion that the energy barrier of the S_E2 reaction would be associated with the energy-level difference ($\Delta E_{\Pi u^*}$) between the π_{u^*} MO level of MCl_2 and the HOMO level of MCl_2 at the TS for the S_E2 reaction (*SI Appendix*, Fig. S10). The $\Delta E_{\Pi u^*}$ is also summarized in Table 1. Here, it is noticeable that the $\Delta E_{\Pi u^*}$ of $FeCl_2$ is larger than that of $CuCl_2$; however, it is lower than those of $CoCl_2$ and $NiCl_2$. In other words, although the energy-lowering effect of the donor–acceptor interaction in $FeCl_2$ is less significant than that in $CoCl_2$ or $NiCl_2$, $FeCl_2$ shows a stronger stabilization effect of the TS by the π_u^*-orbital interaction than that in $CoCl_2$ or $NiCl_2$, which can make

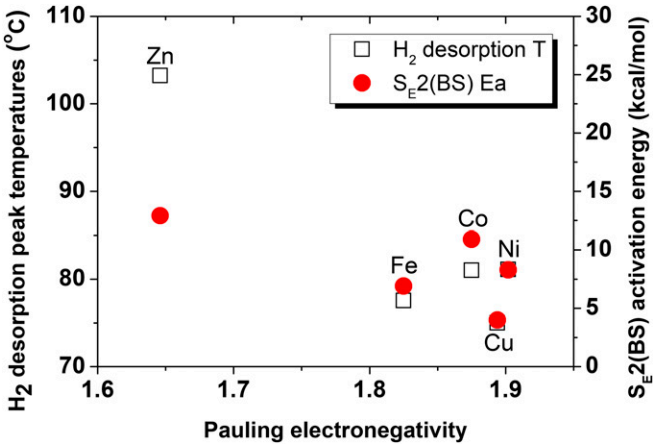

Fig. 2. Correlation between the experimental (29) H_2 desorption peak temperature (left y axis) and the S_E2(BS) activation energy (right y axis) for AB dehydrogenation of various first-row transition-metal chlorides.

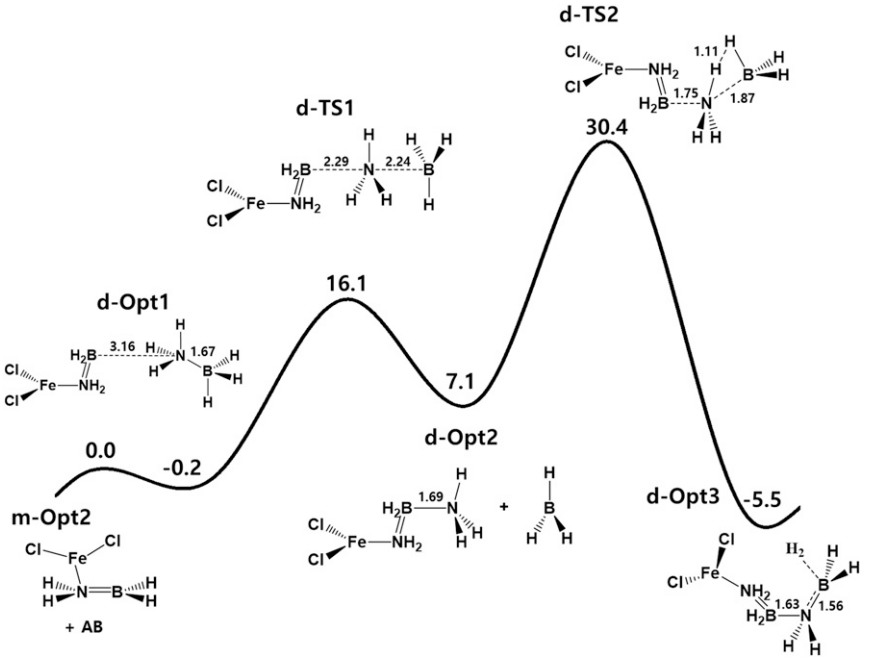

Fig. 3. Calculated reaction pathway for AB dimerization with the help of $FeCl_2$ catalysis, where the DFT-D2 method was used.

the S_E2 reaction barrier with $FeCl_2$ lower than those with $CoCl_2$ and $NiCl_2$. Among the MCl_2 compounds considered in this work, $CuCl_2$ has the highest $\Delta E^{(2)}{}_{N \rightarrow B^*}$ and the lowest $\Delta E_{\Pi u^*}$, which leads to the lowest S_E2 reaction barrier.

Expansion of the S_E2 Reaction to the Polymerization of AB and Other BN Derivatives. Previous experiments reported that after the removal of a single H_2 molecule from AB, NH_2BH_2 oligomers, including dimers, trimers, pentamers, and other intermediates with the empirical formula $(NH_2BH_2)_x$, are generated (7, 35). Zimmerman et al. (36) reported that based on ab initio calculations, amine borane (NH_2BH_2) can serve as an autocatalyst for AB oligomerization by the addition of AB across the B=N double bond of amine borane with an activation energy of 29.5 kcal/mol. However, in the presence of the MCl_2-type catalysts, the AB dimerization and even subsequent polymerization can be explained by the S_E2 reaction framework in a similar manner to that for the monomer, as illustrated in Fig. 1 and *SI Appendix*, Fig. S3. Fig. 3 shows a

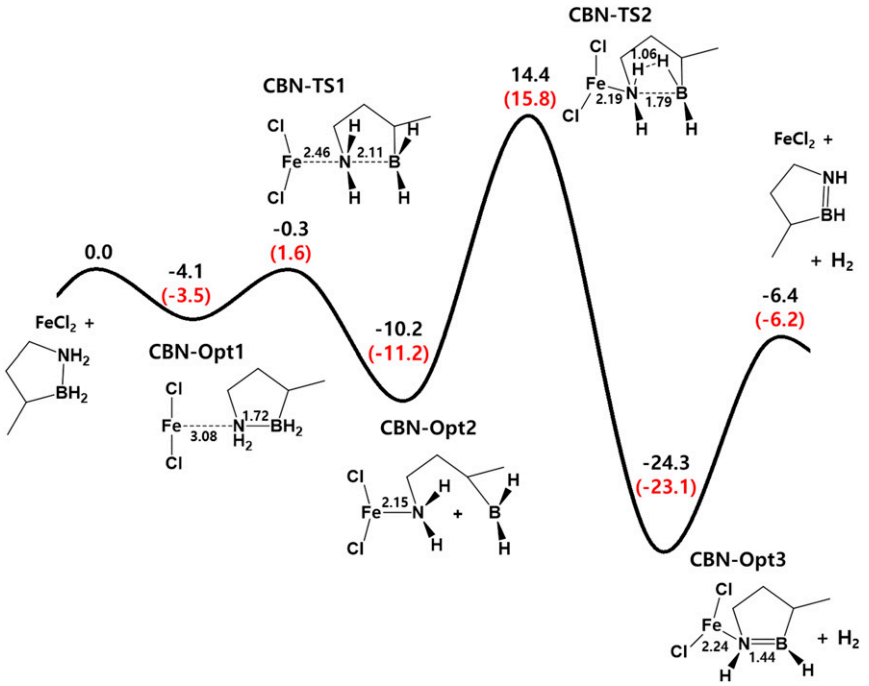

Fig. 4. Calculated reaction pathway for CBN dehydrogenation with the help of $FeCl_2$ catalysis, where the calculation is performed at the DFT-D2 level. Red numbers in parentheses indicate the energies considering the solvent effect.

calculated reaction pathway of AB dimerization with an $FeCl_2$ catalyst through the S_E2 reaction. Following the removal of a single H_2 molecule from AB (m-Opt2 in *SI Appendix*, Fig. S3), the boron atom can become a radical center with a positive partial charge, allowing it to be reused as an electrophile. The boron site in m-Opt2 attacks the nitrogen atom of another AB molecule (d-TS1 structure in Fig. 3), leading to the B–N bond elongation in the AB with an inversion (d-Opt2). The energy barrier for the S_E2 reaction is 16.3 kcal/mol, which is higher than 5.7 kcal/mol in the case of the AB monomer. Here, for the final product (d-Opt3), the geometry of the dimer is not cyclic but rather a twisted zigzag type, which could be regarded as the reason why the quantities of side products are reduced by using MCl_2 catalysts (29).

It is also known that the $FeCl_2$ catalyst improves the dehydrogenation property of the CBN (22); therefore, we have explored the reaction pathway involving the S_E2 reaction in Fig. 4. Overall, the reaction pathway is similar to the case of AB, shown in Fig. 1. The Fe atom in $FeCl_2$ attacks the N center in CBN with simultaneous dissociation of the B–N bond. Despite the hindrance of the carbon backbone, the CBN ring can be opened through the B–N bond dissociation caused by the S_E2(BS) reaction. This reaction is thermodynamically favorable by 14.5 kcal/mol. In particular, the energy barrier for this reaction is as small as 4.4 kcal/mol, which is smaller than that in the case of AB (5.7 kcal/mol) at the same calculation level (DFT-D2). The lower energy barrier in CBN results from the increased repulsive force induced by the eclipsed conformation of the hydrogen atoms between B and N in the TS. The RC_{BN} step is thermodynamically exothermic by 14.1 kcal/mol, and the energy barrier is 24.6 kcal/mol. We denoted the solvation effects on the reaction pathway shown in Fig. 4 by red numbers; however, the effect is not significant.

Conclusion

Thus far, we have elucidated the dehydrogenation mechanism of AB by the MCl_2 catalysts using several ab initio calculation methods. A type of electrophilic substitution reaction in the B–N unit, in particular, an S_E2 type reaction, was found during the catalyzed dehydrogenation reaction of AB catalyzed by MCl_2. The S_E2 reaction determines the catalytic activity of the metal chlorides for the dehydrogenation of AB, as supported by the reported experiments. Interestingly, a similar mechanism is also found in the AB polymerization reaction and even in the dehydrogenation reaction of a BN derivative with a carbon backbone ring (i.e., CBN). This work helps the development of metal-halide catalysts for practical hydrogen storage materials with the BN moiety. We also expect that this work could pave the way for the use of a new reaction in the field of BN chemistry.

Models and Methods

The catalytic effects of various metal chlorides (MCl_2 type, M = 3d- or 4d-transition metals) on the dehydrogenation reactions of AB were investigated with several ab initio calculation methods. To appropriately describe the long-range correlation effect on the substitution reactions occurring during the dehydrogenation, all MCl_2 adducts were fully optimized in the Becke, three-parameter, Lee–Yang–Parr (B3LYP) (37, 38) DFT framework, with the 6–311++G(d,p) basis set (39) plus Grimme's empirical dispersion correction, called the DFT-D2 method (40). A TS for the dehydrogenation reaction was confirmed by the existence of one imaginary frequency, and the zero-point energy correction to the total energy was applied to the total energy.

When higher precision than that available from DFT was required, the CCSD (T) method (41) employing the correlation-consistent triple-ζ plus polarization basis set (42, 43) was applied to the structures fully optimized at the Møller–Plesset second-order perturbation theory (44, 45) level with the same basis set.

Moreover, to explore the relationship between their catalytic effect and electronic structure, we investigated the MO levels of the MCl_2 compounds for the geometries that were fully optimized by CCSD(T). Here, the Stuttgart–Bonn set (SRSC) effective core potential (46) was used for the transition-metal elements. In fact, we also attempted the calculations with the Los Alamos National Laboratory for double zeta quality (LANL2DZ) core potential (47) for transition-metal elements, which has been widely used in the field of organometallic catalysts; however, we found that this approach did not provide a correct energy change for $FeCl_2$ as a function of a multiplicity. The details are explained in *SI Appendix*.

In the case of CBN adducts, a solvation effect was taken into account using the polarized continuum model scheme (48, 49) with a dielectric constant of 2.38 corresponding to the toluene solvent used in a previous experiment (22). In this work, all atomic charges were calculated by the NBO 5.0 scheme (50, 51). All ab initio calculations were performed using the Q-Chem package (52).

ACKNOWLEDGMENTS. This work was supported by Creative Materials Discovery Program through the National Research Foundation of Korea (NRF-2016M3D1A1021140). We acknowledge the financial supports of the Korea Institute of Science and Technology (Grant 2E26940).

1. Sayre LM, Jensen FR (1979) Mechanism in electrophilic aliphatic substitution: A kinetic and stereochemical study of bromodemercuration with bromide ion catalysis. *J Am Chem Soc* 101:6001–6008.
2. Fukuto JM, Jensen FR (1983) Mechanisms of SE2 reactions: Emphasis on organotin compounds. *Acc Chem Res* 16:177–184.
3. Wang PG, et al. (2002) Nitric oxide donors: Chemical activities and biological applications. *Chem Rev* 102:1091–1134.
4. Bruice PY (2007) *Organic Chemistry* (Pearson/Prentice Hall, Upper Saddle River, NJ), 5th Ed, p 796.
5. Wang W, Hellinga HW, Beese LS (2011) Structural evidence for the rare tautomer hypothesis of spontaneous mutagenesis. *Proc Natl Acad Sci USA* 108: 17644–17648.
6. Karkamkar A, Aardahl C, Autrey T (2007) Recent developments on hydrogen release from ammonia borane. *Mater Matters* 2:6–9.
7. Marder TB (2007) Will we soon be fueling our automobiles with ammonia-borane? *Angew Chem Int Ed Engl* 46:8116–8118.
8. Stephens FH, Pons V, Tom Baker R (2007) Ammonia-borane: The hydrogen source par excellence? *Dalton Trans* 25:2613–2626.
9. Eberle U, Felderhoff M, Schüth F (2009) Chemical and physical solutions for hydrogen storage. *Angew Chem Int Ed Engl* 48:6608–6630.
10. Jaska CA, Temple K, Lough AJ, Manners I (2001) Rhodium-catalyzed formation of boron-nitrogen bonds: A mild route to cyclic aminoboranes and borazines. *Chem Commun (Camb)* 11:962–963.
11. Paul A, Musgrave CB (2007) Catalyzed dehydrogenation of ammonia-borane by iridium dihydrogen pincer complex differs from ethane dehydrogenation. *Angew Chem Int Ed Engl* 46:8153–8156.
12. Blaquiere N, Diallo-Garcia S, Gorelsky SI, Black DA, Fagnou K (2008) Ruthenium-catalyzed dehydrogenation of ammonia boranes. *J Am Chem Soc* 130:14034–14035.
13. Heldebrant DJ, et al. (2008) The effects of chemical additives on the induction phase in solid-state thermal decomposition of ammonia borane. *Chem Mater* 20:5332–5336.
14. Yang X, Hall MB (2008) The catalytic dehydrogenation of ammonia-borane involving an unexpected hydrogen transfer to ligated carbene and subsequent carbon-hydrogen activation. *J Am Chem Soc* 130:1798–1799.
15. Käss M, Friedrich A, Drees M, Schneider S (2009) Ruthenium complexes with cooperative PNP ligands: Bifunctional catalysts for the dehydrogenation of ammonia-borane. *Angew Chem Int Ed Engl* 48:905–907.
16. Alcaraz G, Sabo-Etienne S (2010) Coordination and dehydrogenation of amine-boranes at metal centers. *Angew Chem Int Ed Engl* 49:7170–7179.
17. Mal SS, Stephens FH, Baker RT (2011) Transition metal catalysed dehydrogenation of amine-borane fuel blends. *Chem Commun (Camb)* 47:2922–2924.
18. Rossin A, Peruzzini M (2016) Ammonia–borane and amine–borane dehydrogenation mediated by complex metal hydrides. *Chem Rev* 116:8848–8872.
19. Benzouaa R, Demirci UB, Chiriac R, Toche F, Miele P (2010) Metal chloride-doped ammonia borane thermolysis: Positive effect on induction period as well as hydrogen and borazine release. *Thermochim Acta* 509:81–86.
20. Chiriac R, Toche F, Demirci UB, Krol O, Miele P (2011) Ammonia borane decomposition in the presence of cobalt halides. *Int J Hydrogen Energy* 36:12955–12964.
21. Toche F, Chiriac R, Demirci UB, Miele P (2012) Ammonia borane thermolytic decomposition in the presence of metal (II) chlorides. *Int J Hydrogen Energy* 37: 6749–6755.
22. Luo W, Campbell PG, Zakharov LN, Liu SY (2011) A single-component liquid-phase hydrogen storage material. *J Am Chem Soc* 133:19326–19329.
23. Liu Z, Marder TB (2008) B-N versus C-C: How similar are they? *Angew Chem Int Ed Engl* 47:242–244.
24. Bosdet MJD, Piers WE (2009) B-N as a C-C substitute in aromatic systems. *Can J Chem* 87:8–29.
25. Marwitz AJV, Matus MH, Zakharov LN, Dixon DA, Liu S-Y (2009) A hybrid organic/inorganic benzene. *Angew Chem Int Ed Engl* 48:973–977.
26. Campbell PG, Zakharov LN, Grant DJ, Dixon DA, Liu S-Y (2010) Hydrogen storage by boron-nitrogen heterocycles: A simple route for spent fuel regeneration. *J Am Chem Soc* 132:3289–3291.
27. Daly AM, Tanjaroon C, Marwitz AJV, Liu S-Y, Kukolich SG (2010) Microwave spectrum, structural parameters, and quadrupole coupling for 1,2-dihydro-1,2-azaborine. *J Am Chem Soc* 132:5501–5506.

28. Parafiniuk M, Mitoraj MP (2013) Origin of binding of ammonia-borane to transition-metal-based catalysts: An insight from the charge and energy decomposition method ETS-NOCV. *Organometallics* 32:4103–4113.
29. Nakagawa Y, et al. (2016) A systematic study of the effects of metal chloride additives on H2 desorption properties of ammonia borane. *J Chem Eng Data* 61:1924–1929.
30. Pearson RG (1968) Hard and soft acids and bases, HSAB, Part I: Fundamental principles. *J Chem Educ* 45:581–587.
31. Szabó I, Olasz B, Czakó G (2017) Deciphering front-side complex formation in SN2 reactions via dynamics mapping. *J Phys Chem Lett* 8:2917–2923.
32. Grant DJ, Dixon DA (2006) σ- and π-bond strengths in main group 3-5 compounds. *J Phys Chem A* 110:12955–12962.
33. Parafiniuk M, Mitoraj MP (2014) On the origin of internal rotation in ammonia borane. *J Mol Model* 20:2272.
34. Atkins PW (1994) *Physical Chemistry* (Oxford Univ Press, Oxford), 5th Ed, pp 887–888.
35. Böddeker KW, Shore SG, Bunting RK (1966) Boron-nitrogen chemistry. I. Syntheses and properties of new cycloborazanes, (BH2NH2)n1,2. *J Am Chem Soc* 88:4396–4401.
36. Zimmerman PM, Paul A, Zhang Z, Musgrave CB (2009) Oligomerization and autocatalysis of NH2BH2 with ammonia-borane. *Inorg Chem* 48:1069–1081.
37. Lee C, Yang W, Parr RG (1988) Development of the Colle-Salvetti correlation-energy formula into a functional of the electron density. *Phys Rev B Condens Matter* 37:785–789.
38. Becke AD (1993) Density-functional thermochemistry. III. The role of exact exchange. *J Chem Phys* 98:5648–5652.
39. Krishnan R, Binkley JS, Seeger R, Pople JA (1980) Self-consistent molecular orbital methods. XX. A basis set for correlated wave functions. *J Chem Phys* 72:650–654.
40. Grimme S (2006) Semiempirical GGA-type density functional constructed with a long-range dispersion correction. *J Comput Chem* 27:1787–1799.
41. Bartlett RJ, Musiał M (2006) Addition by subtraction in coupled-cluster theory: A reconsideration of the CC and CI interface and the nCC hierarchy. *J Chem Phys* 125:204105.
42. Dunning TH, Jr (1989) Gaussian basis sets for use in correlated molecular calculations. I. The atoms boron through neon and hydrogen. *J Chem Phys* 90:1007–1023.
43. Kendall RA, Dunning TH, Jr, Harrison RJ (1992) Electron affinities of the first-row atoms revisited. Systematic basis sets and wave functions. *J Chem Phys* 96:6796–6806.
44. Møller C, Plesset MS (1934) Note on an approximation treatment for many-electron systems. *Phys Rev* 46:618–622.
45. Head-Gordon M, Head-Gordon T (1994) Analytic MP2 frequencies without fifth-order storage. Theory and application to bifurcated hydrogen bonds in the water hexamer. *Chem Phys Lett* 220:122–128.
46. Dolg M, Wedig U, Stoll H, Preuss H (1986) Energy-adjusted ab initio pseudopotentials for the first row transition elements. *J Chem Phys* 86:866–872.
47. Hay PJ, Wadt WR (1985) Ab initio effective core potentials for molecular calculations. Potentials for K to Au including the outermost core orbitale. *J Chem Phys* 82:299–310.
48. Lange AW, Herbert JM (2010) A smooth, nonsingular, and faithful discretization scheme for polarizable continuum models: The switching/Gaussian approach. *J Chem Phys* 133:244111.
49. Lange AW, Herbert JM (2011) Symmetric versus asymmetric discretization of the integral equations in polarizable continuum solvation models. *Chem Phys Lett* 509:77–87.
50. Glendening ED, Landis CR, Weinhold F (2012) Natural bond orbital methods. *WIREs Comput Mol Sci* 2:1–42.
51. Glendening ED, Landis CR, Weinhold F (2013) NBO 6.0: Natural bond orbital analysis program. *J Comput Chem* 34:1429–1437.
52. Shao Y, et al. (2015) Advances in molecular quantum chemistry contained in the Q-Chem 4 program package. *Mol Phys* 113:184–215.